Commun. Comput. Phys.
doi: 10.4208/cicp.200510.061210a

Vol. **10**, No. 3, pp. 607-634
September 2011

Thermal Response Variability of Random Polycrystalline Microstructures

Bin Wen[1], Zheng Li[1,2] and Nicholas Zabaras[1,*]

[1] *Materials Process Design and Control Laboratory, Sibley School of Mechanical and Aerospace Engineering, Cornell University, Ithaca, NY 14853-3801, USA.*
[2] *State Key Laboratory of Structural Analysis for Industrial Equipment, Faculty of Vehicle Engineering and Mechanics, Dalian University of Technology, Dalian 116024, China.*

Received 20 May 2010; Accepted (in revised version) 6 December 2010

Communicated by Long-Qing Chen

Available online 1 June 2011

Abstract. A data-driven model reduction strategy is presented for the representation of random polycrystal microstructures. Given a set of microstructure snapshots that satisfy certain statistical constraints such as given low-order moments of the grain size distribution, using a non-linear manifold learning approach, we identify the intrinsic low-dimensionality of the microstructure manifold. In addition to grain size, a linear dimensionality reduction technique (Karhunun-Loéve Expansion) is used to reduce the texture representation. The space of viable microstructures is mapped to a low-dimensional region thus facilitating the analysis and design of polycrystal microstructures. This methodology allows us to sample microstructure features in the reduced-order space thus making it a highly efficient, low-dimensional surrogate for representing microstructures (grain size and texture). We demonstrate the model reduction approach by computing the variability of homogenized thermal properties using sparse grid collocation in the reduced-order space that describes the grain size and orientation variability.

AMS subject classifications: 52B10, 65D18, 68U05, 68U07

Key words: Non-linear model reduction, polycrystalline microstructure, homogenization, microstructure reconstruction, stochastic analysis, Karhunun-Loéve Expansion, multiscale modeling, heat conduction.

1 Introduction

Mathematical representation of microstructures is essential in many tasks including the exploration of the process/structure/property triangle [1] and optimizing microstruc-

*Corresponding author. *Email address:* zabaras@cornell.edu (N. Zabaras)

tural topology for achieving optimal properties [2]. In this paper, we are interested in exploring the variability of homogenized thermal properties of microstructures induced by the random nature of the microstructure topology. Computing error-bars of materials properties induced by microstructural uncertainty was examined earlier in [3, 4] using Maximum Entropy methods. The microstructure uncertainty can be introduced in many ways. Here, we assume that we are given a finite set of microstructure snapshots that share some common features, usually in terms of low-order statistical moments of grain size and texture. With this data, we are interested to build a probabilistic model of the underlying random microstructures that share these given statistical features. To efficiently utilize this large scale experimental data, it is important to efficiently compress the data into low-dimensional models.

A polycrystalline microstructure is herein described by its grain size and texture. We are interested in *constructing reduced-order representations of polycrystalline microstructure based on available experimental or simulation-based data* (microstructural snapshots). Given a set of microstructures having the same constituent elements and the same processing history, each microstructure will satisfy some statistical correlations that inherently define its material distribution (volume fraction of one constituent element) and/or the processing history (a specific grain size distribution and/or preferred texture). A reduced-order model that satisfies these statistical correlations while efficiently encoding and quantifying the variations in this data set would significantly accelerate and simplify analysis.

In [5], a (linear) model reduction scheme based on Principle Component Analysis (PCA) was developed for two-phase composite microstructures. However, polycrystalline microstructures contain nonlinear structures that are not captured by PCA. In [6], a nonlinear dimensionality reduction (NLDR) strategy was proposed to embed data variations into a low-dimensional manifold. This methodology was used to construct a reduced-order model of homogenized thermal diffusivity of a two-phase microstructure. Our emphasis here is to extend this NLDR methodology to develop a low-dimensional representation of *polycrystalline microstructures defined in terms of their grain size and texture distribution*. This problem poses significant challenges: (a) reconstruction of microstructures from the low-dimensional space is a difficult task in essence requiring interpolation from the neighboring microstructures while at the same time satisfying all given manifold properties, and (b) NLDR requires a notion of distance between microstructures [6].

Besides the grain size distribution, material properties of polycrystalline microstructures are also highly-dependent on texture. Rodrigues parametrization is often used to describe the orientations of grains. This axis-angle parametrization is convenient when certain symmetries are known in the crystal [7] and therefore a fundamental zone in Rodrigues space exists (e.g., cubic, hcp crystals). The Orientation Distribution Function (ODF) defined in Rodrigues space was used in our earlier work to represent texture [8–10]. If no prescribed information is provided, the orientation of a grain can be totally random. In reality, materials acquire certain preferred texture after processing. This introduces correlations among grain orientations and enable us to perform model reduction techniques on the texture. Some linear approaches have shown success in re-

ducing ODF of cubic crystals when texture samples were known to be collected from a sequence of processes [8–10]. In a general case, the most common representation of an orientation is using Euler angles. In this paper, a discrete microstructure model (n grains) is adopted for an orthotropic material, in which the texture is consisted of finite number of orientations. When a number of snapshots of texture are given, the underlying correlation between the grain orientations can be extracted using the Karhunun-Loéve Expansion. In this manner, a high-dimensional texture representation, constituted of n three-component orientations, can be reduced to a low-dimensional representation, where most properties of the texture samples are preserved. The grain size feature is assumed to be independent of texture. Thus, model reduction can be applied to them independently. After reducing both grain size and texture, the low-dimensional representation of the given microstructure data define a convex hull that can be transformed to a unit hypercube. Any point on this hypercube corresponds to a viable microstructure. Using sparse grid collocation techniques [11], we can sample efficiently this space and generate stochastic interpolants of the microstructure and its material properties of interest.

Our interest here is in computing the variability (e.g., the probability distribution function (PDF)) of thermal conductivity of polycrystalline microstructures whose grain size distribution is given in terms of several moments (e.g., 1st-moment refers to mean volume, 2nd-moment determines standard deviation and higher order moments further constrain the grain size distribution), and its texture is given by a number of samples generated from some random processes. Here, we consider that the property of interest F is a function of grain size distribution and texture, $F(\text{GS,TX})$. We are interested in computing the PDF $P(F)$. The sparse grid collocation method appropriately selects points in the hypercube that correspond to different microstructure realizations. For each of them, one can compute their homogenized properties (e.g., the thermal conductivity) using appropriate multiscale models of thermal diffusion. The sparse grid collocation method hierarchically builds an interpolant for these properties in the random space of grain size and texture. From this interpolant, one can immediately evaluate the property of additional microstructures and using such information construct the PDF through Kernel Density Estimation [12].

The outline of this paper is as follows: In the next section, the central idea of the nonlinear dimension reduction strategy is described. Section 3 introduces a grain size based representation of a microstructure and a methodology for interpolating polycrystal microstructures leading to a viable microstructure that satisfies the statistical grain-distribution correlations. Section 4 introduces the Karhunun-Loéve Expansion on texture space represented by Euler angles. Section 5 briefly reviews the adaptive sparse grid collocation method for solving stochastic PDEs. The anisotropic heat conduction deterministic solver is described in Section 6. Section 7 presents several examples demonstrating the propagation of the microstructural uncertainty in the variability of homogenized thermal conductivity and temperature field of a random microstructure. We conclude in Section 8 with a brief discussion.

2 Model reduction theory

Features of polycrystals are composed of two aspects: topology and texture. The first aspect regards geometry characters, such as grain shape and grain size, while the second is the orientation distribution of grains. For a polycrystalline microstructure, its material properties are mostly determined by grain size and orientation distribution. In order to investigate the property variability of microstructures, both features are considered as random fields. Model reduction techniques are applied to grain size and texture separately, and then their low-dimensional representations are combined to fully represent a microstructure. In this section, focus is on introducing a nonlinear model reduction scheme for the grain size feature. The model reduction on texture is introduced in Section 4.

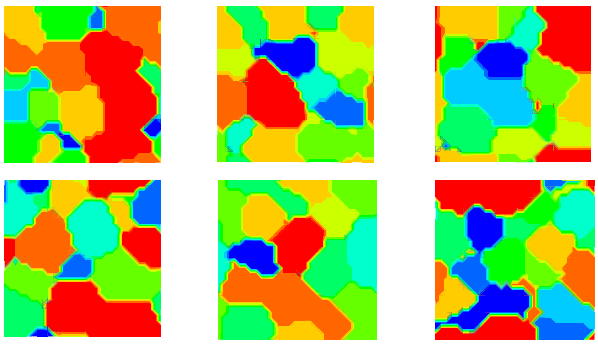

Figure 1: Slices of 3D microstructures satisfying different grain size distribution. (a) constant mean grain size (0.0185mm^3), (b) constant mean grain size (0.0185mm^3) and second-order moment ($3.567\times10^{-4}\text{mm}^6$), and (c) constant grain size (0.0185mm^3), second-order moment ($3.567\times10^{-4}\text{mm}^6$) and third-order moment ($7.265\times10^{-6}\text{mm}^9$).

Fig. 1 shows multiple microstructures that satisfy some given statistics of grain size distribution. Each microstructure that satisfies the given statistics of the grain size distribution is a point that lies on a curve (manifold) embedded in a high-dimensional space. The *manifold learning problem* is as follows: *Given a set of N unordered points belonging to a manifold $\mathcal{M}$ embedded in a high-dimensional space $\mathbb{R}^n$, find a low-dimensional region $\mathcal{A}\subset\mathbb{R}^{d_1}$ that parameterizes $\mathcal{M}$, where $d_1\ll n$.*

In most cases of interest, the manifold is nonlinearly embedded in the input space, making the classical methods of dimensionality reduction (e.g., Principle Component Analysis (PCA), Karhunun-Loéve expansion (KLE), multidimensional scaling (MDS) [13]) highly approximate. We focus our attention in the current work to non-linear dimension reduction [14–17]. We will consider the global methods of non-linear dimension reduction and in particular using the Isomap and its numerous variants which attempt to preserve geometry at all scales. They ensure that nearby points on the manifold (with distance defined via a suitable metric) map to nearby points in the low-dimensional

space and faraway points map to faraway points in the low-dimensional space. The distance between original points is identical to that between their low-dimensional counterparts. Geodesic distances reflect the true low-dimensional geometry of the manifold. The geodesic distance between two points on a manifold can be intuitively understood to be the shortest distance between the two points *along the manifold*.

Subsequent to the construction of the geodesic distance between the sample points $\{\mathbf{x}_i\}$ in the high-dimensional space, the Isomap [16] algorithm constructs the low-dimensional parametrization as a set of points $\{\mathbf{y}_i\}$ in a low-dimensional space that most accurately preserve the geodesic distance. With the Isomap algorithm, *given a set of N-unordered points belonging to a manifold $\mathcal{M}$ embedded in a high-dimensional space $\mathbb{R}^n$, a low-dimensional region $\mathcal{A}\in\mathbb{R}^{d_1}$ is computed which is isometric to $\mathcal{M}$, with $d_1\ll n$.* We approximate the geodesic distance using the concept of graph distance $\mathcal{D}_G(i,j)$. This approximation, $\mathcal{D}_G(i,j)$, asymptotically matches the actual geodesic distance $\mathcal{D}_M(i,j)$ in the limit of large number of samples [6]. Since the important feature we are looking to embed and recreate is the grain size distribution, we choose this feature to define our distance metric (see Section 3).

Having computed the pairwise distance matrix between the given microstructures, one can compute the location of N points in a reduced-order surrogate space, $\mathbf{y}_i\in\mathbb{R}^{d_1}$ such that the distance between these points is arbitrarily close to the given distance matrix. Multi Dimensional Scaling (MDS) allows this mapping [6]. The intrinsic dimension d_1 of an embedded manifold is linked to the rate of convergence of the length-functional of the minimal spanning tree of the geodesic distance matrix of the unordered data points in the high-dimensional space [6]. The rate of change of the length functional as more number of points are chosen is related to the dimensionality of the manifold via a simple relation $\log(L)=a\log(N)+\epsilon$, where $a=(d_1-1)/d_1$. The intrinsic dimensionality, d_1, can be estimated by finding the length functional for different number of samples N and subsequently finding the best fit for a.

The procedure above results in N points in a low-dimensional space $\mathbb{R}^{d_1}$ and a low-dimensional convex region $\mathcal{A}\subset\mathbb{R}^{d_1}$, given as $\mathcal{A}=\text{convex hull}(\mathbf{y}_i)$. We consider that all possible microstructures that satisfy the given constraints are equiprobable. One can then map the convex hull $\mathcal{A}$ to a unit hypercube with the same dimensionality d_1. Every point in the hypercube corresponds to a point on $\mathcal{A}$ and thus after reconstruction to a microstructure in $\mathcal{M}$. Since microstructures are equiprobable, we consider each of the dimensions of the hypercube as defining an independent uniform random variable. These random variables define our stochastic support space. $\mathcal{A}$ serves as the surrogate space of $\mathcal{M}$. We can access the variability in $\mathcal{M}$ by sampling over $\mathcal{A}$, or equivalently the hypercube, which is the sampling space in the sparse grid collocation method [11]. The microstructure reconstruction $\mathcal{A}\rightarrow\mathcal{M}$ will be discussed in Section 3.2. The overall steps of the procedure are summarized in Fig. 2. The sparse grid collocation method has been shown to be an efficient method that uses deterministic solvers of e.g., deformation, diffusion, flow, etc. in heterogeneous (but deterministic) media, to compute the varying response and homogenized properties of random microstructures.

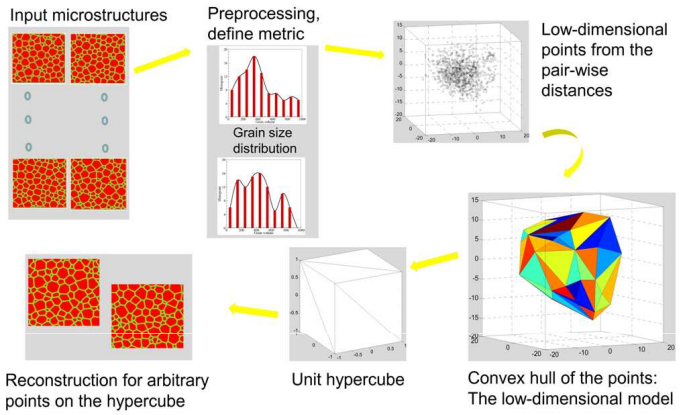

Figure 2: The various steps in a data-driven model reduction of polycrystal microstructures. The high-dimensional microstructures are mapped to a low-dimensional region $\mathcal{A}$. This convex region is mapped to a unit hypercube. Each sampling point on this hypercube corresponds to a microstructure that needs to be reconstructed using the given data. The sparse grid collocation method uses samples from the hypercube (thus microstructures) to create interpolants of properties of random microstructures.

3 Microstructure representation and reconstruction methodologies

3.1 Microstructure representation: grain size vector of a microstructure

The high-dimensional representation of a microstructure topology feature in this paper is chosen to be the grain size distribution, namely the volume of grains. A polycrystalline microstructure contains finite number of grains and each grain has its own size. If the size of each grain is given, the microstructure is not uniquely determined. The only differences in geometry of these microstructures are the shape and arrangement of the grains, which have less influence on the material properties in comparison to grain size. We treat microstructures having the same grain size distribution to be the same (or more accurately belonging in the same class). Given a vector containing the size information of each grain, we can construct realizations of the microstructure using a grain growth method [18]. In this paper, the microstructure representation is chosen as the grain size (in terms of grain volume) vector sorted by ascending order (we refer to it as the "sorted grain size vector"). In the following, the grain size will be described in terms of the voxel numbers belonging to each grain. This facilitates the grain growth method for constructing a digital model of microstructures. For example, let us consider a cubic microstructure that contains 4 grains whose volumes are given as $\mathbf{GS}=\{30,20,40,10\}$ pixels. Rearranging the grain size in ascending order, the new representation of this microstructure is $\mathbf{GS}=\{10,20,30,40\}$. This resulting vector is chosen as the representation of this kind of microstructure. After being sorted, microstructures belonging to the same class result in the same grain size vector, while different classes give different vectors. This microstructure representation is selected as it is easy to express and satisfy the

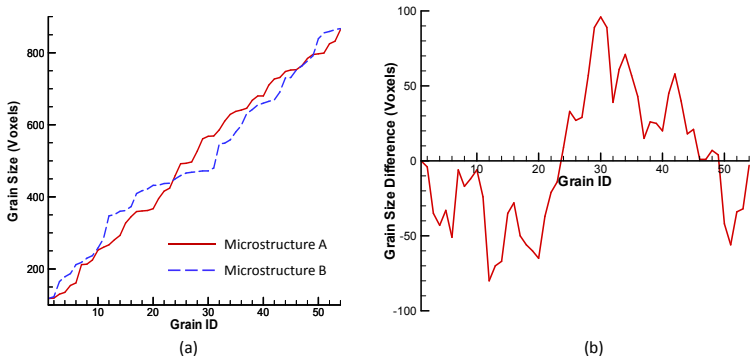

Figure 3: (a) Microstructure measurement represented by sorted grain size vector. (b) The difference between the two microstructures.

given constraints on grain size (mean, standard deviation, higher-order moments, etc.) and in addition, the (non-unique) reconstruction of a microstructure with given moment constraints on the grain size distribution is rather straightforward using the phase field method. To estimate the difference between two microstructures $\mathbf{A}\in\mathcal{M}$ and $\mathbf{B}\in\mathcal{M}$, we first sort their grain sizes by ascending order and then measure their distance $\mathcal{D}_G(\mathbf{A},\mathbf{B})$ as follows:

$$\mathcal{D}_G(\mathbf{A},\mathbf{B})=\Big(\sum_i^n (GS_i^A-GS_i^B)^2\Big)^{\frac{1}{2}}. \tag{3.1}$$

Fig. 3 shows an example of using sorted grain size vector to measure the difference between two 54-grain microstructures. Fig. 3(a) depicts the sorted grain volume distribution of two microstructures having the same mean grain size. Fig. 3(b) measures the difference in each grain between the microstructures, which also tells how much microstructure **A** is different from microstructure **B**. The dimension of this grain size vector is determined by the number of grains in the microstructure. For a microstructure containing 54 grains, the dimensionality of its representation is $n=54$ dimensional. As the mean size is fixed, there are only 53 independent dimensions. If more constraints are added, the dimensionality will be further reduced.

3.2 Microstructure reconstruction

Given a set of samples $\{\mathbf{x}_i\}$, $i=1,\cdots,N$, in grain size feature space $\mathcal{M}$, the non-linear dimension reduction strategy (Section 2) converts these points into a set of points $\{\mathbf{y}_i\}$, $i=1,\cdots,N$ belonging to a convex set $\mathcal{A}\subset\mathbb{R}^{d_1}$ defining the reduced representation of the space of microstructures. As $\mathcal{A}$ is the surrogate space of $\mathcal{M}$, one can access the complete variability in the topology and property distribution of grain size in $\mathcal{M}$ by simply sampling over the region $\mathcal{A}$. For a useful reduced-order model of the microstructure space, an explicit mapping $\mathcal{F}^{-1}$ from $\mathcal{A}$ to $\mathcal{M}$ has to be constructed.

As shown in Fig. 2, the reduced-dimensionality space $\mathcal{A}$ is used as the surrogate space from which acceptable microstructures need to be sampled (at arbitrary points). The

procedure of reconstructing a microstructure (here we mean the grain size feature of a microstructure) $\mathbf{x}\in\mathcal{M}$ from the low-dimensional space $\mathcal{A}\subset\mathbb{R}^{d_1}$ is as follows: (1) select a point in the low-dimensional space $\mathbf{y}\in\mathcal{A}$, (2) find the m nearest neighbors of $\mathbf{y}$ and denote them as $\mathbf{y}_i$, $i=1,\cdots,m$, (3) find the microstructures $\mathbf{x}_i$, $i=1,\cdots,m$ in the high-dimensional space $\mathcal{M}\subset\mathbb{R}^n$ that are corresponding to $\mathbf{y}_i$, $i=1,\cdots,m$. Based on isometry, $\mathbf{x}$ could be computed following a linear interpolation algorithm:

$$\mathbf{x}=\sum_{i=1}^{m}W_i\mathbf{x}_i,\qquad W_i=\frac{1}{\mathcal{D}(\mathbf{y}_i,\mathbf{y})}\Big[\sum_{j=1}^{m}\frac{1}{\mathcal{D}(\mathbf{y}_j,\mathbf{y})}\Big]^{-1}. \tag{3.2}$$

Note that the distance metric between nearest neighbors in the reduced space $\mathcal{A}\subset\mathbb{R}^{d_1}$ is the Euclidean distance and the points $\mathbf{x_i}\in\mathcal{M}$ were the sorted grain size vectors defined earlier. The above equation demonstrates that the new generated grain size vector can be interpolated by its nearest neighbors weighed by the reciprocal distances between their corresponding low-dimensional points. The mean grain size of the interpolated microstructure automatically equals the required value because of the linearity of Eq. (3.2). However, when the microstructures on the manifold are constrained by higher-order moments, the resulted microstructure by interpolation cannot satisfy all the constraints, which means it slightly deviates from the manifold. To compute a microstructure satisfying all the given moments, we need to modify the grain sizes obtained with Eq. (3.2). This procedure is referred to as projecting the image onto the manifold [6].

An algorithm that can adjust the grain size distribution to satisfy constraints on the second and third moment of the grain size distribution is briefly described below. Controlling grain size distribution satisfying the second-order moment is straightforward. Given a grain size vector whose mean size is M_1, we would like to adjust the grain sizes so that its second-order moment is M_2. To do this, we first transform the original grain size vector to one that has zero mean by subtracting M_1 from each component. We then weight each component with the ratio of the expected standard deviation to current standard deviation. The algorithm is as follows:

Step 1. $E_1=\frac{1}{n}\sum_{i=1}^{n}S_i=M_1$;

Step 2. $S_i=S_i-M_1$;

Step 3. $E_2=\frac{\sum_{i=1}^{n}S_i^2}{n}$;

Step 4. $a=\sqrt{\frac{M_2-M_1^2}{E_2}}$;

Step 5. $S_i=aS_i$.

Having the zero-mean grain size vector satisfying the expected standard deviation, the final grain size vector that satisfies both the mean size and second-order moment can be obtained by adding M_1 to its components, i.e., $S_i=M_1+aS_i$, for $i=1,\cdots,n$.

The control the third-order moment is more complicated. Two iterative processes are needed to accomplish this task. The basic idea is to find an intersection vector of two

surfaces. One surface is composed of microstructures satisfying the first two moments and the other one is defined by the third-order moment M_3. Still, the mean size M_1 is subtracted from the grain size vector. The first three target moments of the zero mean grain size vectors are then equal to $\hat{M}_1=0$, $\hat{M}_2=M_2-M_1^2$, and $\hat{M}_3=M_3-3M_1M_2+2M_1^3$, respectively. The complete algorithm is as follows:

Step 1. $\hat{S}_i=S_i-M_1$;

Step 2. $\hat{S}'_i=\hat{S}_i$, and $E_1=\frac{1}{n}\sum_{i=1}^n S_i$;

Step 3. $\hat{S}_i=\hat{S}_i-E_1$;

Step 4. $E_2=\frac{1}{n}\sum_{i=1}^n S_i^2$;

Step 5. $\hat{S}_i=\hat{S}_i\sqrt{\frac{\hat{M}_2}{E_2}}$;

Step 6. loop

- $\delta_i=\frac{3\hat{S}_i^2}{n}$;
- $d=\sum_{i=1} n\delta_i^2$, $E_3=\frac{1}{n}\hat{S}_i^3$;
- $m=\hat{M}_3-E_3$;
- $\hat{S}_i=\hat{S}_i+\frac{m}{d}\delta_i$;
- if $|m|<$cutoff, break;

Step 7. error$=$norm$(\hat{S}'_i-\hat{S}_i)$;

Step 8. if error$<$cutoff, go to Step 9, else go to Step 1;

Step 9. $S_i=M_1+\hat{S}_i$, $i=1,\cdots,n$.

The grain size vector $\{S_i, i=1,\cdots,n\}$ now satisfies the three given moment constraints.

Given a set of grain size vectors satisfying the prescribed constraints, realizations of polycrystalline microstructures can be constructed. This is an essential step to allow us to compute their thermal or other properties. Techniques commonly used to generate microstructures are based on the phase-field and level set methods, and on Voronoi tessellations. In this work, we utilize first the Voronoi tessellation method to give an approximate microstructure with grain sizes that nearly satisfy the expected distribution. Then using this microstructure as a starting point, we utilize the phase field method as a smoothing operation to optimize the initial microstructure forcing it to better satisfy the desired grain size distribution. The grain size is measured by the number of voxels within each grain.

To generate a Voronoi tessellation that results in microstructures close to the desired grain distribution, we follow the work in [19]. The algorithm implemented makes enough space for each grain while minimizing the "competition" between neighboring grains. For a microstructure $\mathbf{M}$, we denote the ith grain as $\mathbf{M}(i)$, its size as $\mathbf{M}(i)\cdot GS$, and the coordinates of its nucleus is $\mathbf{M}(i)\cdot\mathbf{x}$. First the microstructure domain is populated with points whose coordinates are sampled using a quasi-random sequence (the Sobel

sequence). This sequence ensures that newly sampled points maximally avoid the points sampled before. The number of points, which indicates the number of grains, is decided by the expected mean grain size of the microstructure: $n=Size(\mathbf{M})/E(\mathbf{M}(i)\cdot GS)$. Assuming all the grains are spheres in 3D (or circles in 2D), we can compute the desire radius $M(i)\cdot r$ of each grain region from its expected size $\mathbf{M}(i)\cdot GS$. Let $d=dis(\mathbf{M}(i)\cdot\mathbf{x},\mathbf{M}(j)\cdot\mathbf{x})$ being the distance between the nuclei of two grains $\mathbf{M}(i)$ and $\mathbf{M}(j)$, and $a=\mathbf{M}(i)\cdot r+\mathbf{M}(j)\cdot r$. The forcing function between grains is then defined as

$$\mathbf{F}(i,j)=\begin{cases} 0, & d>a, \\ \mathbf{n}(j,i)(a-d), & \text{otherwise}, \end{cases} \tag{3.3}$$

where $\mathbf{F}(i,j)$ is the force exerted by point j on point i along the direction $\mathbf{n}(j,i)$ which starts at j and points at i. Minimizing the sum of all the forces exerting on all the grains with respect to the Voronoi nuclei locations will lead to a proper (based on the desired grain sizes) space for each grain. This optimization problem is solved in a periodic domain using a conjugate gradient approach with line search. After updating the points using the forcing function defined above, a Voronoi cell tessellation is computed using these points as the centers.

Voronoi tessellations, however, cannot provide a microstructure that exactly satisfies the desired grain size distribution. The phase-field method [18, 20, 21] is introduced to smooth the resulting microstructure so that the expected grain size distribution can be accurately achieved. In a phase-field model, the grain boundary is approximated as a diffuse interface. At each point $\mathbf{r}$ in the microstructure, a finite number of continuous order parameters (i.e., field variables) $\rho_q(\mathbf{r},t)$, $q=1,\cdots,Q$ are defined at a given time t. The total free energy F of the microstructure is defined as the function of the field variables and their gradients. The growth dynamics of the phase field approach drives, as the simulation proceeds, the total free energy to approach its minimum, where only a single field variable within each grain takes a value of 1 while all others are 0. The main process of simulating grain growth with a phase-field method proceeds as follows:

1. Initialize $\rho_q(\mathbf{r},t)$,$q=1,\cdots,Q$ on each node $\mathbf{r}$ in a grid at $t=0$.
2. Using the time-dependent Ginzburg-Landau equations, compute:

$$\frac{\partial\rho_q(\mathbf{r},t)}{\partial t}=-L_q\frac{\partial F}{\partial\rho_q}=-L_q\Big(-\alpha\rho_q+\beta\rho_q^3+2\gamma\rho_q\sum_{s\neq q}^{G}\rho_s^2-\kappa_q\nabla^2\rho_q\Big),\quad q=1,\cdots,Q. \tag{3.4}$$

3. Update the value of $\rho_q(\mathbf{r},t)$ on the next time step

$$\rho_q(\mathbf{r},t+\Delta t)=\rho_q(\mathbf{r},t)+\frac{\partial\rho_q(\mathbf{r},t)}{\partial t}\Delta t. \tag{3.5}$$

4. If $t<T_{\max}$ go to Step 2, else the simulation is complete.

If state q leads to the highest value of $\rho_q(\mathbf{r},t)$ at position $\mathbf{r}$, then the state q will be the one assigned to location $\mathbf{r}$. Here the parameters: $\alpha,\beta,\gamma,\kappa_q,L_q$ are chosen as: $\alpha=\beta=\gamma=1$, $\kappa_q=0.5$, $L_q=1$, see [18,20,21]. To control the grain sizes during the grain growth process, we dynamically change the parameter α that makes the only positive contribution to the growth of ρ_q. For a grain q, we take α as the ratio of its desired size to its temporary size on each time step. When the current size of the grain is smaller than the desired size, then α will be larger than 1, and the grain q will grow larger. The opposite effect will take place when $\alpha<1$. Notice that, when we change the parameter α, the value of $\rho_q(\mathbf{r},t)$ may not be limited between 0 and 1. For this reason, normalization of $\rho_q(\mathbf{r},t)$ is performed via

$$\rho_q(\mathbf{r},t)=\frac{\rho_q(\mathbf{r},t)}{\sum_{i=1}^{Q}\rho_i(\mathbf{r},t)}.$$

To initialize the phase field smoothing process, we use the resultant model from the Voronoi tessellation algorithm. Denote $V(\mathbf{r})$ the grain ID at location $\mathbf{r}$. $V(\mathbf{r})$ should be an integer such that $1\leq V(\mathbf{r})\leq G$. Then field variables are set as

$$\rho_q(r,0)=\begin{cases}0, & q\neq V(\mathbf{r}),\\ 1, & q=V(\mathbf{r}).\end{cases} \tag{3.6}$$

If there are $Q=G$ variables of $\rho_q(r,t)$ on each position, the computational cost will be extremely high. Thus, a sparse data structure of storing the variables $\rho_q(r,t)$ as proposed in [22] is adopted. Finally, we note that although the phase field approach alone (without using the Voronoi tessellation method for initialization) can be used to directly obtain a microstructure satisfying the desired grain size distribution, the method initialized with a coarse Voronoi tessellation structure is found to be much more efficient. The microstructure will serve as the finite element model to the deterministic solver, so that the thermal

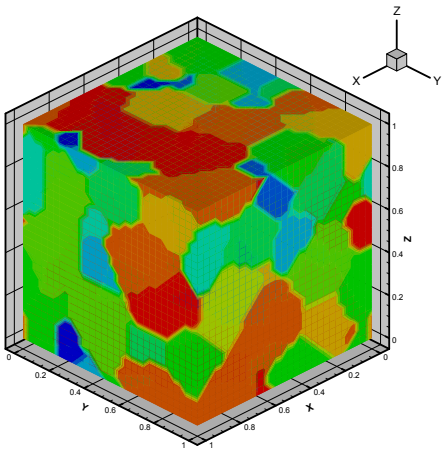

Figure 4: A realization of microstructure containing 54 grains (mean volume is 500 voxels). The total voxel number of the microstructure domain is 27000.

properties of the polycrystal can be analyzed. A visualization of a microstructure having 54 grains is shown in Fig. 4, where the total voxel number is 27000 and only the mean grain size is constrained to be 500 voxels.

4 Texture modeling

Besides grain size, the properties of anisotropic materials are highly dependent on their texture. For the case of discrete microstructure containing moderate number of grains, the texture effect is usually much more significant than the grain size effect. To examine the effect of variability in texture on the property of the microstructure, the texture is defined as a random field, whose variables are orientations of individual grains. In this paper, the orientation of a grain is defined by a series of rotations around its crystal coordinate axes, which are known as the Euler angles: $\{\phi,\theta,\psi\}$. Coordinate system is a composition of rotations from a reference frame. If a property tensor in the local (crystal) coordinate system is given as $\mathbf{K}_L$, then its representation in global (microstructural) coordinate system is

$$\mathbf{K}_G=\mathbf{R}\mathbf{K}_L\mathbf{R}^T, \tag{4.1}$$

where $\mathbf{R}$ is the rotation matrix defined as

$$\mathbf{R}=\mathbf{B}\mathbf{C}\mathbf{D}. \tag{4.2}$$

$\mathbf{B},\mathbf{C},\mathbf{D}$ correspond to three rotations illustrated in Fig. 5.

$$\mathbf{D}=\begin{bmatrix}\cos\phi & \sin\phi & 0\\ -\sin\phi & \cos\phi & 0\\ 0 & 0 & 1\end{bmatrix},\quad \mathbf{C}=\begin{bmatrix}1 & 0 & 0\\ 0 & \cos\theta & \sin\theta\\ 0 & -\sin\theta & \cos\theta\end{bmatrix},\quad \mathbf{B}=\begin{bmatrix}\cos\psi & \sin\psi & 0\\ -\sin\psi & \cos\psi & 0\\ 0 & 0 & 1\end{bmatrix}. \tag{4.3}$$

Writing the Euler angles of all the grains in a vector format, we can define the texture of a microstructure as

$$\boldsymbol{\tau}=\left\{\phi^1,\theta^1,\psi^1,\phi^2,\theta^2,\psi^2,\cdots,\phi^n,\theta^n,\psi^n\right\}^T, \tag{4.4}$$

where n is the total number of grains.

Considering the symmetry of orthorhombic, tetragonal and cubic crystals, the fundamental interval of Euler angles can be reduced as

$$\phi\sim U[0,\pi],\qquad \theta\sim U[0,\pi],\qquad \psi\sim U[0,\pi]. \tag{4.5}$$

Here, we assume that our texture samples are obtained from a random process, which results in microstructures with texture that are close to certain preferred pattern, but with certain perturbation. Assume the target texture is specified as a deterministic one. The texture samples can then be modeled by adding a white noise to each of the components of the target. For example, let the target texture be $\boldsymbol{\tau}_0=\left\{\phi_0^1,\theta_0^1,\psi_0^1,\cdots,\phi_0^n,\theta_0^n,\psi_0^n\right\}^T$. The components of texture sample $\boldsymbol{\tau}_i$ can then be modeled as

$$\phi_i^j=\phi_0^j+\epsilon_\phi^j,\qquad \theta_i^j=\theta_0^j+\epsilon_\theta^j,\qquad \psi_i^j=\psi_0^j+\epsilon_\psi^j, \tag{4.6}$$

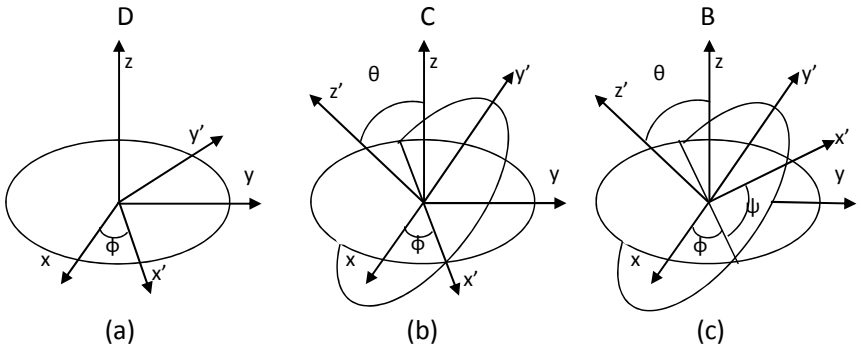

Figure 5: Three Euler rotations. (a) The first rotation is by an angle ϕ about the z-axis using **D**, (b) the second rotation is by an angle $\theta\in[0,\pi]$ about the former x-axis (now x') using **C**, and (c) the third rotation is by an angle ψ about the former z-axis (now z') using **B**.

where $i=1,\cdots,N$ is the texture sample ID, $j=1,\cdots,n$ is the grain ID in the texture. In the above equations, the ϵ's are sampled independently from a Gaussian distribution $N(0,\sigma^2)$. By repeating this process, N new texture samples $\boldsymbol{\tau}_j$, $j=1,\cdots,N$ are obtained that are used as the texture input model for stochastic analysis. Notice that all three Euler angles obtained by Eq. (4.6) are within the interval $[0,\pi]$. Thus, these angles are in a one-to-one relationship with their corresponding cotangent values. To facilitate model reduction on texture samples, instead of using the Euler angles directly, we represent the orientation of each grain i as:

$$\tau_j^{i_1}=\cot(\phi_j^i),\qquad \tau_j^{i_2}=\cot(\theta_j^i),\qquad \tau_j^{i_3}=\cot(\psi_j^i). \tag{4.7}$$

It has been observed that these transformed texture samples can be more effectively reduced by the Karhunun-Loéve Expansion (KLE). Given a set of texture samples, the unbiased estimate of the covariance matrix of these texture vectors is

$$\tilde{\mathbf{C}}=\frac{1}{N-1}\sum_{i=1}^{N}(\boldsymbol{\tau}_i-\bar{\boldsymbol{\tau}})^T(\boldsymbol{\tau}_i-\bar{\boldsymbol{\tau}}),\qquad \bar{\boldsymbol{\tau}}=\frac{1}{N}\sum_{i=1}^{N}\boldsymbol{\tau}_i. \tag{4.8}$$

$\boldsymbol{\tau}_i$ is the i-th realization of $\boldsymbol{\tau}\in\mathcal{T}$, and N is the total number of known realizations, namely the sample number. The truncated Karhunun-Loéve Expansion of the random vector $\boldsymbol{\tau}$ is then written as

$$\boldsymbol{\tau}(\mathbf{r},\boldsymbol{\omega})=\bar{\boldsymbol{\tau}}(\mathbf{r},\boldsymbol{\omega})+\sum_{i}^{d_2}\sqrt{\lambda^i}\boldsymbol{\phi}^i(\mathbf{r})\eta^i(\boldsymbol{\omega}), \tag{4.9}$$

where $\boldsymbol{\phi}^i$, λ^i are the i-th eigenvector and eigenvalue of $\tilde{\mathbf{C}}$, respectively; $\{\eta^i(\boldsymbol{\omega})\}$ is a set of uncorrelated random variables having the following two properties

$$E(\eta^i(\boldsymbol{\omega}))=0,\quad E(\eta^i(\boldsymbol{\omega})\eta^j(\boldsymbol{\omega}))=\delta_{ij},\quad i,j=1,\cdots,d_2, \tag{4.10}$$

and their realizations are obtained by

$$\eta_j^i = \frac{1}{\sqrt{\lambda^i}}\left\langle \boldsymbol{\tau}_j - \bar{\boldsymbol{\tau}}, \boldsymbol{\phi}^i \right\rangle, \quad j=1,\cdots,N,\ i=1,\cdots,d_2, \tag{4.11}$$

where $\langle\cdot,\cdot\rangle$ denotes the scalar product in $\mathbb{R}^n$. Since the covariance function is symmetric and positive definite, all the eigenvalues are positive real numbers and the eigenvectors are mutually orthogonal and they span the space in which $\boldsymbol{\tau}(\mathbf{r},\boldsymbol{\omega})$ belongs to. The summation in Eq. (4.9) is mean square convergent and usually truncated after few dominant terms, which preserves most information of the vector $\boldsymbol{\tau}$.

The truncated realizations of $\{\boldsymbol{\eta}_j\} \in \Gamma \subset \mathbb{R}^{d_2}$ are treated as reduced texture representations, which is analogous to the reduced grain size samples $\{\mathbf{y}_i\} \in \mathcal{A}$. The only constraint that we know about the random variables $\{\boldsymbol{\eta}_j\}$ is from Eq. (4.10). Without assuming any other information, the distribution of $\boldsymbol{\eta}$ should satisfy the uncorrelated constraints while as close as possible to the uniform distribution. This distribution can be easily derived using Maximum Entropy Principle (MaxEnt) [10] and is well known as the uncorrelated Gaussian distribution with mean vector $\{\mathbf{0}\}$ and correlation matrix $\mathbf{I}$. Only in very few special cases, the uncorrelated Gaussian distribution random variables are not independent [23] and our example is not in that category. Therefore, here we treat $\boldsymbol{\eta}$ as a set of independent random variables that are normally distributed around $\mathbf{0}$. A convenient method to transform $\boldsymbol{\eta}$ to random variables $\boldsymbol{\zeta}$ that are uniformly distributed within the hypercube $[0,1]^{d_2}$ is the Rosenblatt transformation [24]. The distribution of $\boldsymbol{\zeta}$ is in fact the cumulative distribution functions (CDF) of $\boldsymbol{\eta}$

$$\zeta_1 = \Phi_{\eta^1}(\eta^1), \tag{4.12a}$$

$$\zeta_2 = \Phi_{\eta^2|\eta^1}(\eta^2|\eta^1) = \Phi_{\eta^2}(\eta^2), \tag{4.12b}$$

$$\vdots$$

$$\zeta_{d_2} = \Phi_{\eta^{d_2}|\eta^1\cdots\eta^{d_2-1}}(\eta^{d_2}|\eta^1\cdots\eta^{d_2-1}) = \Phi_{\eta^{d_2}}(\eta^{d_2}), \tag{4.12c}$$

where $\Phi(\cdot)$ is the standard normal CDF and in current case is

$$\Phi_{\eta^i}(\eta^i) = \frac{1}{2}\left[1 + erf\left(\frac{\eta^i}{\sqrt{2}}\right)\right]. \tag{4.13}$$

For a given point in the hypercube $\boldsymbol{\zeta} \in [0,1]^{d_2}$, its corresponding point $\boldsymbol{\eta}$ from the original distribution is naturally found to be

$$\eta^i = \Phi^{-1}(\zeta_i), \qquad i=1,\cdots,d_2, \tag{4.14}$$

which can be immediately recovered to a texture vector using Eq. (4.9). The corresponding Euler angles are obtained through inversion of Eqs. (4.7).

Based on the analysis above, each microstructure $\mathbf{h}(\mathbf{x},\boldsymbol{\tau})$ (with both grain size and texture features) that belongs to high-dimensional stochastic space $\mathcal{H} = \mathcal{M} \times \mathcal{T}$, now, can

be presented by $\mathbf{l}(\mathbf{y},\boldsymbol{\eta})$ in the low-dimensional surrogate space $\mathcal{L}=(\mathcal{A}\times\Gamma)\subset\mathbb{R}^d$ ($d=d_1+d_2$).

Remark 4.1. In this work, we have decoupled the grain size and texture effects. In fact, one can assign any orientation to any grain. Indeed this is the source of the grain size effect in our work in [19]. This grain size/texture coupling effects will introduce an additional variation into the macroscopic response of the microstructure and this will not easily allow us to identify the individual effects of grain size or texture. Treating the grain size and texture as correlated variables is of course an important approach to be considered.

A mapping from $\mathcal{L}$ to $\mathcal{H}$ can be constructed for sampling allowable microstructure features. Define the stochastic model for the feature variation as $\mathcal{F}^{-1}(\boldsymbol{\xi}):\mathcal{L}\to\mathcal{H}$, where $\boldsymbol{\xi}=\{\xi_1,\cdots,\xi_d\}$ is a random vector chosen from $\mathcal{L}$. This low-dimensional stochastic model $\mathcal{F}^{-1}$ for the microstructure is the input to the SPDEs defining the thermal diffusion problem of interest in this paper. For grain size feature, this mapping is described in Section 3.2; for texture, the mapping is directly performed by Eq. (4.9), where $\mathcal{F}^{-1}(\boldsymbol{\eta}):\boldsymbol{\eta}\to\boldsymbol{\tau}$.

Mapping the low-dimensional representation to a hypercube having the same dimensionality [6], the uncertainty of the thermal property of the microstructure can be efficiently investigated using the Adaptive Sparse Grid Collocation (ASGC) method. It is a stochastic collocation procedure that solves stochastic partial differential equations (SPDEs) by computing the solution at various sample points, $\boldsymbol{\xi}$, from this space, $\mathcal{L}$. Each of the sample points corresponds to a microstructure that can be interrogated to evaluate its thermal response. The space grid collocation approach will then create an interpolant of the thermal response in the d-dimensional stochastic space of random microstructures.

5 Sparse grid collocation

In the previous sections, the grain size and texture of a polycrystalline microstructure have been reduced to a set of lower dimensional representations that will serve as the input to the stochastic simulation. A highly efficient, stochastic collocation based solution strategy is used to solve for the thermal response. This section briefly reviews the adaptive sparse grid collocation method for solving SPDEs. For details, the interested reader is referred to [11].

The basic idea of sparse grid collocation is to approximate the multi-dimensional stochastic space $\mathcal{L}$ using interpolating functions on a set of collocation points $\{\boldsymbol{\xi}_i\}_{i=1}^M\in\mathcal{L}$. The collocation method collapses the multi-dimensional problem (based on the Smolyak algorithm) to solving M (M is the number of collocation points) deterministic problems. One computes the deterministic solution at various points in the stochastic space and then builds an interpolant function that best approximates the required solution. Notice, during the process, the mapping $\mathcal{F}^{-1}$ from the low-dimensional surrogate $\mathcal{L}$ space to the high-dimensional microstructure space $\mathcal{H}$ needs to be implemented, so that the deterministic (heat conduction) solver can be used.

In the context of incorporating adaptivity, the Newton-Cotes grid is utilized with equidistant support nodes. A hierarchical basis is used in constructing the interpolant. The function of interest $u(t,\boldsymbol{\xi})$ can be approximated by

$$\hat{u}_{d,q}(t,\boldsymbol{\xi}) = \sum_{\|\mathbf{i}\|\leq d+q} \sum_{\mathbf{j}\in B_i} \omega_{\mathbf{j}}^{\mathbf{i}}(t)\cdot a_{\mathbf{j}}^{\mathbf{i}}(\boldsymbol{\xi}). \tag{5.1}$$

The mean of the random solution is evaluated as:

$$E(\hat{u}_{d,q}(t)) = \sum_{\|\mathbf{i}\|\leq d+q} \sum_{\mathbf{j}\in B_i} \omega_{\mathbf{j}}^{\mathbf{i}}(t)\cdot \int_{\mathcal{L}} a_{\mathbf{j}}^{\mathbf{i}}(\boldsymbol{\xi}) d\boldsymbol{\xi}, \tag{5.2}$$

where q is the depth (level) of sparse grid interpolation and d is the dimensionality of stochastic space. B_i is a multi-index set. $\omega_{\mathbf{j}}^{\mathbf{i}}$ is the hierarchical surplus, which is the difference between the function value $u(t,\boldsymbol{\xi})$ at the current point $\boldsymbol{\xi}$ and interpolation value $\hat{u}_{d,q-1}(t,\boldsymbol{\xi})$ from the coarser grid in the previous level. $a_{\mathbf{j}}^{\mathbf{i}}$ is the d-dimensional multilinear basis functions defined by tensor product. For the estimation of higher-order moments (k-th order) of the function of interest, we only need to change u to u^k. The function of interest u and its interpolation $\hat{u}$ in the current work are the temperature of each point of the microstructure and the homogenized effective thermal conductivity of the microstructure.

With increasing level of interpolation, new support nodes are added if the error indicator

$$\gamma_{\mathbf{j}}^{\mathbf{i}} = \frac{\|\omega_{\mathbf{j}}^{\mathbf{i}}\cdot\int_{\mathcal{L}} a_{\mathbf{j}}^{\mathbf{i}}(\boldsymbol{\xi})d\boldsymbol{\xi}\|_{L_2}}{\|E_{\|\mathbf{i}\|-d-1}\|_{L_2}} \tag{5.3}$$

is larger than the threshold ϵ. The new collocation points will be generated locally in the next level. The error indicator $\gamma_{\mathbf{j}}^{\mathbf{i}}$ measures the contribution of each term in Eq. (5.2) to the integration (mean) value relative to the overall integration value computed from the previous interpolation level.

After the ASGC has been performed, the thermal response (temperature field and homogenized effective thermal conductivity) of random microstructures is obtained. Using the high-dimensional interpolant of the homogenized thermal conductivity, one can compute statistical quantities of interest such as realizations, moments and the probability density function (PDF) using kernel density estimation [12].

6 Deterministic solver

The physics of interest in the current work is the variability of macroscopic thermal conductivity and temperature distribution of anisotropic polycrystalline microstructures due to the uncertainty in grain size and texture. The deterministic solver solves a steady-state heat conduction problem using the finite element method (FEM) and calculates the effective thermal conductivity of the microstructure. The heat conduction is governed by the

generalized Fourier's Law of anisotropic materials, which (without heat generation) can be written as

$$\nabla\cdot\left(\mathbf{K}\nabla T\right)=0, \tag{6.1}$$

where $\mathbf{K}$ is the thermal conductivity tensor and T the temperature field. In isotropic materials, $\mathbf{K}$ is a diagonal matrix with three identical components. Therefore, it can be treated as a scalar. However, in the case of anisotropic materials, the thermal conductivity varies in different directions. To compute the thermal conductivity in certain direction of a crystal, the crystal orientation is required to be known. Suppose the thermal conductivity tensor of a single crystal is $\mathbf{K}'$ in its local coordinate system, which is rotated by $\mathbf{R}$ according to the reference coordinates. The transformed conductivity tensor $\mathbf{K}$ of this crystal in the global (microstructural) coordinates is then calculated from Eq. (4.1). $\mathbf{K}=\mathbf{R}\mathbf{K}'\mathbf{R}^T$ is the conductivity represented in the sample coordinate system. The weak form of the governing equation can be written as

$$\int_\Omega \nabla w^T\mathbf{K}\nabla T dV=-\int_{\Gamma_q}\bar{\mathbf{q}}w ds, \tag{6.2}$$

in which, $w=0$ on the boundary where Dirichlet condition (specified temperature) is prescribed and Γ_q is the boundary where Neumann condition (specified flux) is applied.

Solving this heat conduction equation by the FEM, the temperature field and flux can be found over the microstructure domain. The effective thermal conductivity tensor $\mathbf{K}_{eff}$ of the entire microstructure is defined by

$$\langle\mathbf{K}\nabla T\rangle=\mathbf{K}_{eff}\langle\nabla T\rangle, \tag{6.3}$$

where

$$\langle f\rangle=\frac{1}{\mathcal{V}}\int_{\mathcal{V}} f dV \tag{6.4}$$

is the volume average of f over the microstructure domain. In practice [25], one solves Eq. (6.3) by considering three different cases in which a temperature gradient is imposed via temperature boundary conditions in the $\mathbf{x}$, $\mathbf{y}$, and $\mathbf{z}$, respectively. Denote these solutions by $T_j, j=1,\cdots,3$. Then for this case, we can write Eq. (6.3) as follows:

$$\langle\mathbf{K}\nabla T_1\rangle=\mathbf{K}_{eff}\langle\nabla T_1\rangle,\quad \langle\mathbf{K}\nabla T_2\rangle=\mathbf{K}_{eff}\langle\nabla T_2\rangle,\quad \langle\mathbf{K}\nabla T_3\rangle=\mathbf{K}_{eff}\langle\nabla T_3\rangle. \tag{6.5}$$

These equations can be used to compute the effective conductivity $\mathbf{K}_{eff}$. The developed deterministic solver is applicable to any materials having ortho-symmetry, such as tetragonal, orthorhombic or/and cubic crystals. An example of 3D tetragonal symmetric Tin microstructure (Fig. 4) is considered to verify the reliability of the deterministic solver. A unit cubic ($volume=1\text{mm}^3$) microstructure with 54 grains is meshed by $29\times29\times29$ brick elements. The thermal conductivity along the three orthogonal lattice directions are $k_a=0.0742\text{Wmm}^{-1}K^{-1}$, $k_b=0.0742\text{Wmm}^{-1}K^{-1}$, $k_c=0.0515\text{Wmm}^{-1}K^{-1}$, see [26]. Three different boundary conditions are applied to compute the effective thermal conductivity

tensor. In each case, the temperature on both sides along one of the directions (**x**, **y**, or **z**) is fixed at $0.5^{\circ}C$ and $-0.5^{\circ}C$, respectively. All other boundaries are kept insulated. With this manner, a linear system of equations with the 9 components (only 6 independent values because of symmetry) of the effective conductivity tensor as the unknowns can be constructed and solved. Assigning random texture to the microstructure, the computational effective thermal conductivity is

$$\mathbf{K}_{eff} = \begin{bmatrix} 0.068071 & -0.000538 & 0.000120 \\ -0.000538 & 0.067672 & -0.000435 \\ 0.000120 & -0.000435 & 0.062403 \end{bmatrix} \mathrm{Wmm}^{-1}\mathrm{K}^{-1}. \tag{6.6}$$

The diagonal components are close to the experimental value ($0.0666\mathrm{Wmm}^{-1}\mathrm{K}^{-1}$) and simulation value ($0.0684\mathrm{Wmm}^{-1}\mathrm{K}^{-1}$) given in [26]. Notice that the effective thermal conductivity tensor is symmetric positive definite. The temperature field and flux distribution of the microstructure when the temperature boundary condition is applied in the **y** direction are plotted in Fig. 6. As expected, the flux in the **y** direction is larger than in the other two directions. However, due to anisotropy, the fluxes in the **x** and **z** directions cannot be neglected.

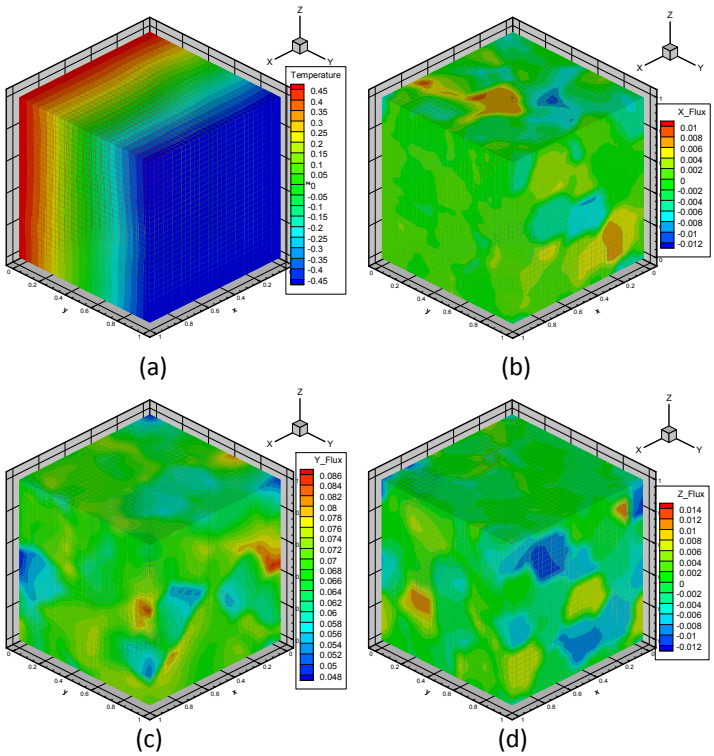

Figure 6: (a) Temperature field of Tin microstructure given temperature boundary conditions. (b) Flux field of Tin microstructure in the **x** direction. (c) Flux field of Tin microstructure in the **y** direction. (d) Flux field of Tin microstructure in the **z** direction.

Since $\mathbf{K}_{eff}$ is a function of the microstructure configuration (grain size and texture), given various microstructures that share some statistical features, a stochastic diffusion problem can be solved to predict the temperature variability on the underlying random microstructures. For this task, we employ the sparse grid collocation method.

7 Numerical examples

In this section, several examples are presented to study the statistics of thermal response and variability of conductivity of polycrystalline microstructures based on the model reduction techniques and sparse grid collocation method introduced earlier. The statistics of the temperature field and the distribution of the effective thermal conductivity over the microstructure domain are of interest. The deterministic solver uses the finite element anisotropic polycrystal heat conduction model introduced in the previous section. The macroscopic effective thermal conductivity tensor is evaluated by Eq. (6.5). In the following numerical examples, Tin, having Tetragonal symmetry, is studied. The methodology is also applicable to other materials such as orthorhombic or cubic polycrystals. The thermal conductivity along the three lattice directions are $k_a = 0.0742\text{Wmm}^{-1}\text{K}^{-1}$, $k_b = 0.0742\text{Wmm}^{-1}\text{K}^{-1}$, $k_c = 0.0515\text{Wmm}^{-1}\text{K}^{-1}$, see [26]. The microstructure of interest is a unit (edge length $1mm$) cube with grains satisfying certain constraints. The boundary conditions considered are the same as those in Section 6.

The methodologies used in solving this stochastic problem are the combination of the algorithms presented in the previous sections. The overall algorithm is summarized below:

1. Generate a number of grain size samples $\{\mathbf{x}_i\} \in \mathcal{M}, i = 1, \cdots, N$ according to certain information (prescribed mean size, 2nd- and 3rd-order moments, etc).
2. Utilize NLDR to reduce the dimensionality of the grain size samples. Their low-dimensional representations are $\{\mathbf{y}_i\} \in \mathcal{A}, i = 1, \cdots, N$. The optimal dimensionality of the lower space $\mathcal{A}$ is linked to the rate of convergence of the length functional of the minimal spanning tree of the geodesic distance matrix of the unordered data points in the high-dimensional space. A convex hull is constructed as the envelope of these data points in the reduced dimensionality space.
3. Generate texture samples consisting of Euler angles using for example a random process. Perform KLE on these texture samples, $\{\boldsymbol{\tau}_i(\boldsymbol{\omega})\}$, $i = 1, \cdots, N$. The low-dimensional representations $\{\boldsymbol{\eta}_i\} \in \Gamma$ can be obtained by truncating the eigen-spectrum to a desired level.
4. Combine the reduced grain size and texture to form the low-dimensional surrogate of feature space of microstructures, which is the stochastic input to the sparse grid collocation SPDE solver.
5. Use ASGC method to construct the stochastic solution. This method solves the deterministic problem at various collocation points $\boldsymbol{\xi}$ on the stochastic space and constructs an interpolation based approximation to the stochastic solution. For a given set of stochastic collocation points, the corresponding microstructures of these points can be found (by the mapping $\mathcal{F}^{-1}: \mathcal{L} \to \mathcal{H}$) and used as inputs in the solution of the SPDEs. For each of these deterministic problems,

the thermal response is computed by FEM for anisotropic polycrystalline materials. The ASGC method constructs the stochastic interpolant of the thermal response using the deterministic responses for the appropriately selected sparse grid collocation points.

6. After the corresponding stochastic thermal problem has been solved, the homogenized effective thermal conductivity for any other microstructure realization in the stochastic support space can be calculated using the hierarchical interpolating functions. The probability distribution of the homogenized effective thermal conductivity is constructed using kernel smoothing density estimation on the histogram of realizations.

7.1 Example 1

In the first example, the effect of the grain size constraints on the microstructure thermal property distribution is examined. One thousand microstructure samples are first generated. Each sample contains 54 grains whose volume is uniformly distributed in the interval between 100 and 900 voxels. The mean grain volume of each microstructure is controlled to be 500 voxels, while higher-order moments are free to vary. These samples are used as the input database of grain size feature. By applying the NLDR method (Section 2), we first construct the geodesic distance matrix between points and then map them to a low-dimensional space through Multi-Dimensional Scaling (MDS) and Isomap. The number of nearest neighbors is set to be 10. The intrinsic dimensionality d_1 of the low-dimensional space is estimated by linking to the convergence of the length functional of the minimal spanning tree (MST) of the neighborhood graph defined by geodesic distance matrix [6]. To be specific, for various sizes of samples (varying from 20 to 1000), points were randomly picked from the set of samples. The minimal spanning tree of these sample sets was computed. The length functional of the MST was computed for each of these sample sets. The optimal dimensionality of the low-dimensional set is related to the slope of the line representing the relationship between the length functional and the sample number (in Logarithm form). The slope is computed using a least squares fit and found to be a=0.6973. The reduced dimensionality is estimated using $d_1=1/(1-a)$ (Section 2), which is rounded to $d_1=3$. In this way, the original 54 dimensional grain size representation is reduced to 3.

The prescribed texture samples are generated following the technique introduced in Section 4. A texture sample i is obtained by adding a Gaussian perturbation to each of the components of the deterministic one. In this example, we assume that the variance of the noise is $\sigma^2=0.01$:

$$\phi_i^j=\phi_0^j+\epsilon_\phi^j, \qquad \theta_i^j=\theta_0^j+\epsilon_\theta^j, \qquad \psi_i^j=\psi_0^j+\epsilon_\psi^j, \tag{7.1}$$

where

$$\epsilon_\phi^j\sim N(0,0.01), \qquad \epsilon_\theta^j\sim N(0,0.01), \qquad \epsilon_\psi^j\sim N(0,0.01).$$

The unbiased estimate of the covariance matrix $\tilde{\mathbf{C}}$ is constructed. We apply KLE (Section 4) using the covariance matrix and set the energy cutoff to be 90%-truncate the eigenvalue and eigenvector number d_2 when the "energy" captured by the first d_2 eigenvalues

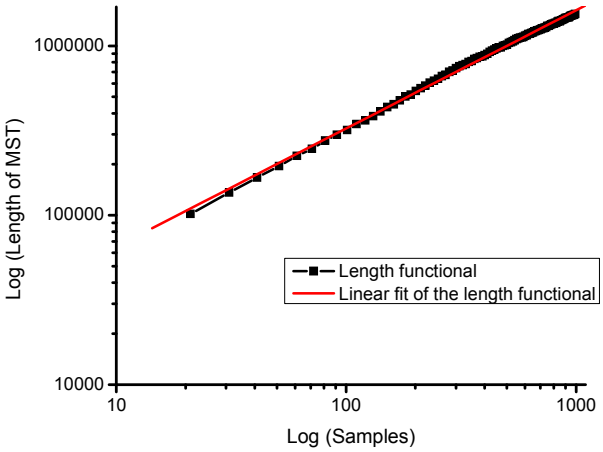

Figure 7: Plot of the length functional of the MST with respect to various sample sizes.

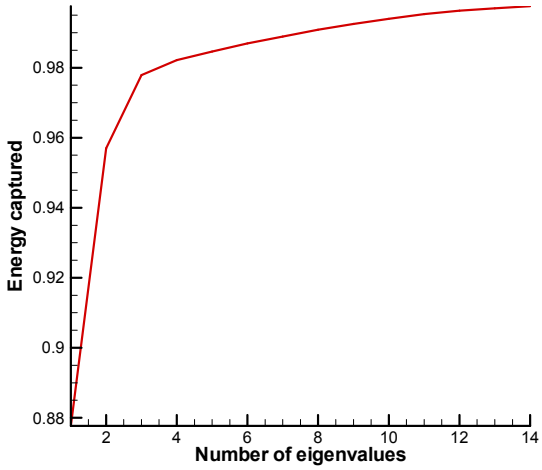

Figure 8: The "energy" captured by the most significant eigenvalues.

is larger than 90%, $\sum_{i=1}^{d_2}\lambda^i/\sum_{i=1}^{n}\lambda^i \geq 90\%$. Fig. 8 shows that the first 2 eigenvalues of the covariance matrix captured 95.7% of the total "energy" (sum of all eigenvalues). Therefore, the reduced dimensionality needed to describe the initial texture is 2.

Combining the information from the grain size and texture and assuming they are independent from each other, we finally map the microstructure features to a five-dimensional unit hypercube $[0,1]^5$, see [6]. The first 3 dimensions of the hypercube correspond to grain size and the last 2 dimensions correspond to texture features. Adaptive sparse grid collocation (ASGC) is utilized to investigate the thermal property uncertainty due to the variation of grain size and texture. During this process, collocation nodes are generated in the hypercube adaptively. Each node can be mapped to a microstructure feature set (Sections 3.2 and 4). Given the grain size distribution, a real microstructure

model can be generated using the grain growth method (Section 3.2). The thermal response of the new microstructure is then simulated utilizing the anisotropic polycrystal heat conduction FEM deterministic solver (Section 6).

The variables of interest are the temperature at each node, as well as the homogenized effective conductivity of the microstructure. Setting the control error (Eq. (5.3)) to be 0.001, 4915 collocation points are adaptively generated through 7 levels. The computed temperature field and effective thermal conductivities converge at interpolation level 7 (the maximum error indicator of all the collocation nodes is smaller than the specified criterion 0.001). As mentioned, the ASGC method decomposes the multi-dimensional stochastic problem into the solution of a number of deterministic problems. Thus, the deterministic solver is called at each collocation point to estimate the thermal response. The mean temperature field of the microstructure during this process is plotted in Fig. 9. The computed mean effective conductivity tensor estimated by Eq. (5.2) using the ASGC is

$$\mathbf{K}_{eff}=\begin{bmatrix} 0.067618 & -0.001147 & 0.001705 \\ -0.001147 & 0.068098 & 0.000956 \\ 0.001705 & 0.000956 & 0.062777 \end{bmatrix} \mathrm{Wmm}^{-1}\mathrm{K}^{-1}. \tag{7.2}$$

Constructing the interpolation for the 6 independent components of the macroscopic effective thermal conductivity tensor, we can obtain the distribution of them by sampling uniformly from the hypercube. According to Eq. (5.1), given a point located in the hypercube, a corresponding effective conductivity tensor can be evaluated. We generate sufficient samples (in this case, 10000 points are generated from the interpolant), and then the histogram of the effective conductivities can be obtained. Utilizing kernel smoothing density estimation [12], the PDF of the effective thermal conductivity is plotted in Fig. 10. From Fig. 10, we can observe that the diagonal conductivities are concentrated around $0.065\mathrm{Wmm}^{-1}\mathrm{K}^{-1}$, while the off-diagonal around 0. In addition, the distribution of the diagonal components is wider then that of the off-diagonal components.

Microstructures satisfying higher-order moment constraints are examined next. We first constrain the second-order moment of grain size to be 260000, while the mean size is maintained at 500. A convex hull having 114 faces is constructed. The texture is taken to be the same as in the earlier case. Applying the ASGC up to level 7, 4725 collocation points are adaptively generated when the error indicators converge to less than 0.001. The mean temperature field of the microstructure is similar to that shown in Fig. 9. The computed mean effective conductivity tensor estimated by Eq. (5.2) using the ASGC is

$$\mathbf{K}_{eff}=\begin{bmatrix} 0.068032 & -0.001036 & 0.000933 \\ -0.001036 & 0.068115 & 0.001013 \\ 0.000933 & 0.001013 & 0.062261 \end{bmatrix} \mathrm{Wmm}^{-1}\mathrm{K}^{-1}, \tag{7.3}$$

which does not significantly differ from the values computed earlier. The distribution of the effective thermal conductivity is plotted in Figs. 12(a) and (b).

Finally, the microstructures are constrained by 3 moments. The 3rd-order moment is set to be 143000000, while keeping the other grain size constraints as in the earlier case.

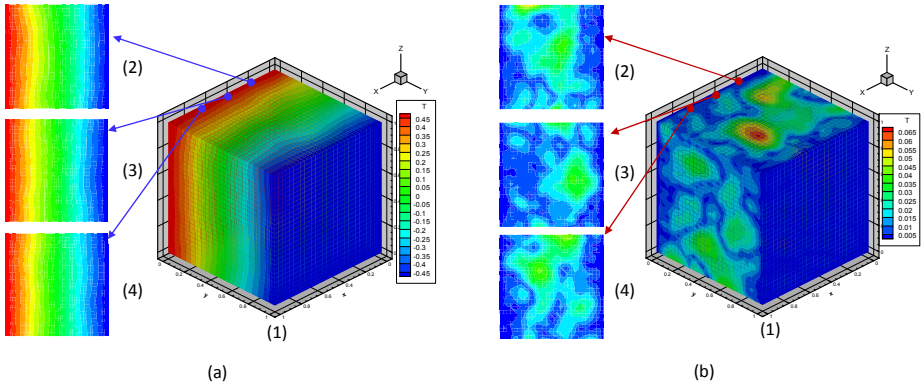

Figure 9: (a) (1) Mean temperature field of microstructures satisfying specific constraints on grain size and texture distributions. The temperature on the boundaries perpendicular to $\mathbf{y}$ direction is fixed. (2)-(4) are the slice plots at $x=0.25,0.5$, and 0.75 (b) (1) The standard deviation of the temperature distribution. (2)-(4) are the slice plots at $x=0.25,0.5$, and 0.75.

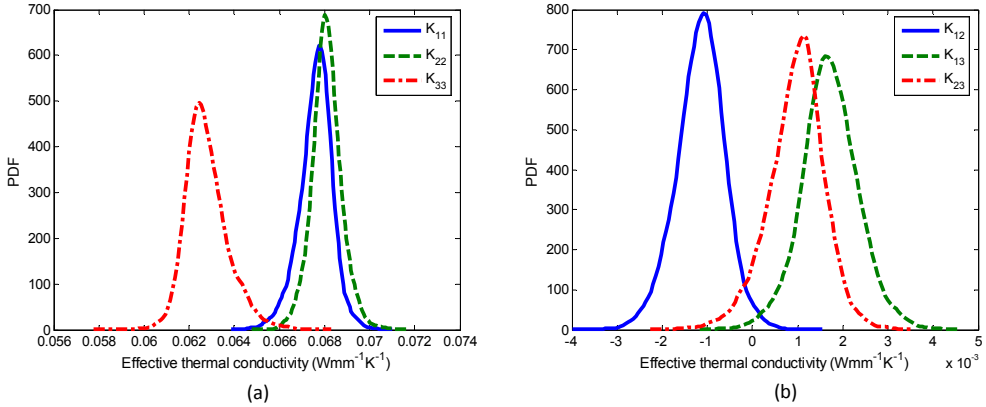

Figure 10: Macroscopic effective thermal conductivity distributions of microstructures whose mean grain size is fixed. (a) Diagonal components; (b) Off-diagonal components.

In this case, most grain sizes in the microstructure are close but smaller than the mean size, while a few grain sizes are much larger than the others. If the third-order moment is set to a higher value, the variation of the grain sizes from sample to sample is quite small and thus the resulting microstructures tend to have the same grain size vector. A comparison of sorted grain size vectors among three microstructure samples whose grain size distributions are constrained by different number of moments is demonstrated in Fig. 11. We can observe that the microstructure constrained by only the mean grain size tends to have almost evenly distributed grain sizes. Grain sizes of the case constrained by two moments are more concentrated around the mean size. In the case that three moments are constrained, most grain sizes are a little smaller than the mean size, while a couple of grains have unusually large values.

A convex hull having 100 faces is constructed for the grain size feature. Without varying the texture distribution, 4690 deterministic problems are adaptively solved in ASGC.

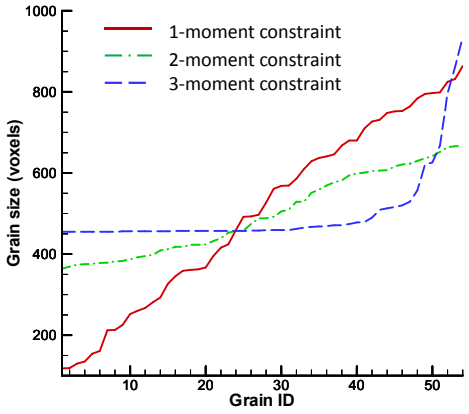

Figure 11: Three microstructure samples whose grain size distributions are constrained by different number of moments. The first one is constrained by mean volume 500; the second is constrained by the same mean volume and the second-order moment 260000; the last one is constrained by a third-order moment 143000000 in addition to the first two constraints.

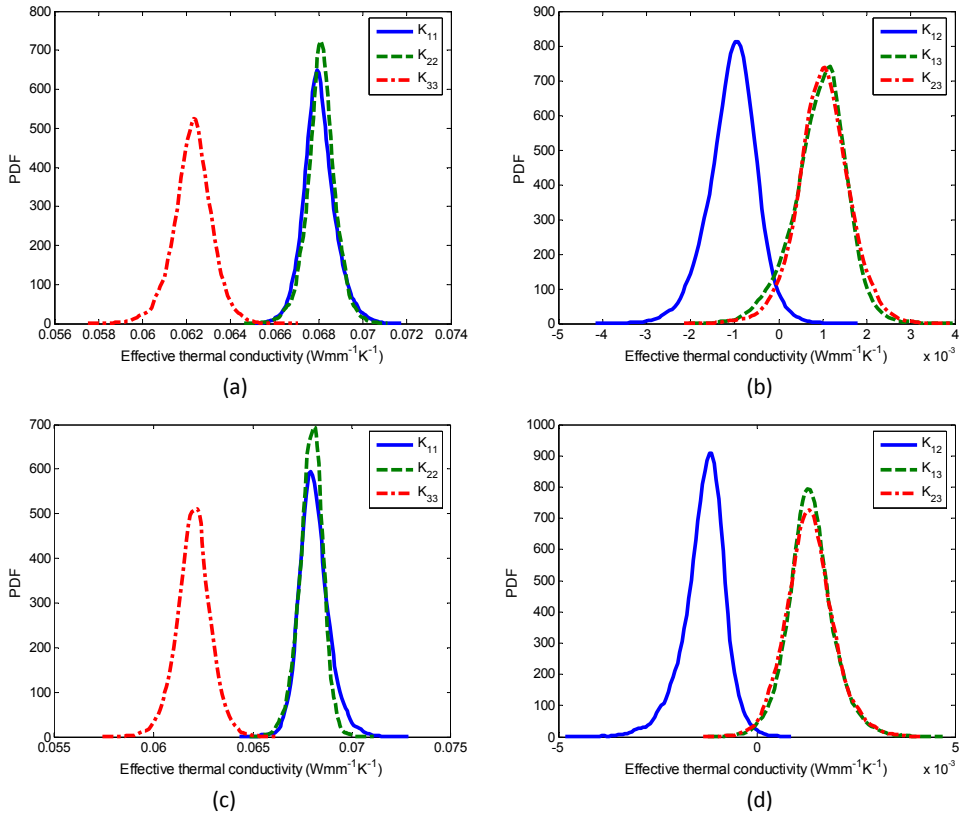

Figure 12: Macroscopic effective thermal conductivity distributions of microstructures satisfying higher-order grain size constraints. (a) Diagonal components when first 2 moments are constrained; (b) Off-diagonal components when the first 2 moments are constrained. (c) Diagonal components when the first 3 moments are constrained; (d) Off-diagonal components when the first 3 moments are constrained.

The mean effective thermal conductivity tensor is computed from the ASGC algorithm to be

$$\mathbf{K}_{eff} = \begin{bmatrix} 0.068096 & -0.001329 & 0.001368 \\ -0.001329 & 0.067939 & 0.001342 \\ 0.001368 & 0.001342 & 0.062023 \end{bmatrix} \text{Wmm}^{-1}\text{K}^{-1}. \tag{7.4}$$

The distribution of the effective thermal conductivity is also plotted in Figs. 12(c) and (d).

From Figs. 10 and 12, we can observe that the effective conductivity distributions are very close to each other in these three cases. When higher grain size moments are constrained, the thermal conductivity distributions tend to be a little narrower. This implies that higher-order grain size moments will change the thermal property of microstructures to some extent but do not have significant effect.

7.2 Example 2

The second example examines the texture effect on the microstructure effective thermal conductivity. The grain size samples are only constrained by mean grain size, which is equal to 500 voxels. However, the orientation variation in texture samples is larger than in the first example. Maintaining the original deterministic texture unchanged, we increase the transformed Euler angles variance from 0.01 to 0.09:

$$\epsilon_{\phi}^{j} \sim N(0,0.09), \qquad \epsilon_{\theta}^{j} \sim N(0,0.09), \qquad \epsilon_{\psi}^{j} \sim N(0,0.09). \tag{7.5}$$

Performing KLE on the texture samples, a set of 3-dimensional representations are generated. The "energy" captured by the first 3 eigenvalues is 96.8%. Using the ASGC method up to level 7 with 10082 adaptively computed realizations, the mean macroscopic effective thermal conductivity distribution is estimated to be

$$\mathbf{K}_{eff} = \begin{bmatrix} 0.068312 & -0.000393 & 0.000501 \\ -0.000393 & 0.067750 & 0.000534 \\ 0.000501 & 0.000534 & 0.061710 \end{bmatrix} \text{Wmm}^{-1}\text{K}^{-1}. \tag{7.6}$$

Sampling from the hypercube $[0,1]^6$, the effective thermal conductivity distribution is constructed and plotted in Figs. 13(a), and (b). We can observe that the distribution of the effective thermal conductivity is broadened.

The mean temperature fields for these two situations in which the texture variation is larger demonstrate more evidently the anisotropy than the first example as shown in Fig. 14.

8 Conclusions

In this paper, the effect of multiple sources of uncertainties on the macroscopic thermal conductivity of polycrystal microstructures is studied. A microstructure was considered

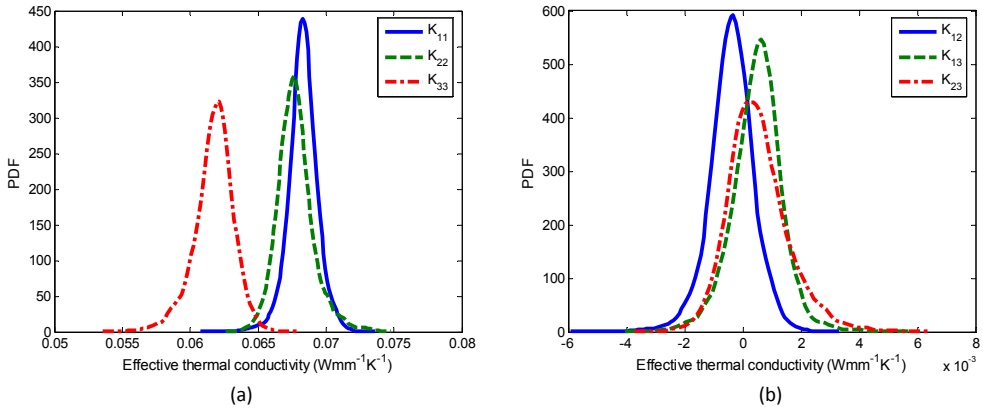

Figure 13: Macroscopic effective thermal conductivity distributions of microstructures with larger texture uncertainty.

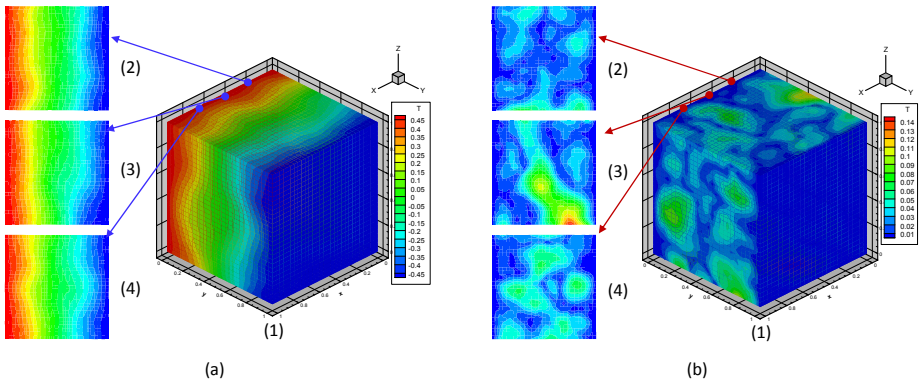

Figure 14: (a) Mean temperature field of microstructures having intermediate large texture uncertainty; (b) Mean temperature field of microstructures having large texture uncertainty.

as a combination of random fields consisted of grain size and texture. Given a set of microstructure samples as the realization of these random fields, dimensionality reduction techniques were applied to find their underlining correlations. A nonlinear model reduction based on Isomap was performed on grain size and a linear Karhunun-Loéve Expansion is applied for texture. Adaptive sparse grid collocation was then introduced to sample new microstructures from the low-dimensional space and to produce an interpolant in the stochastic space of the thermal response and effective conductivity. The thermal response of the microstructures satisfying given information was computed using a FEM based anisotropic heat conduction model and the effective thermal conductivity distribution is constructed. The effect of texture and grain size randomness is studied. We have shown that the model reduction techniques greatly simplified the representation of random microstructure features, while their significant features can be preserved. The computed variability of the effective (homogenized) thermal conductivity provides

important guidance in the analysis and design of random heterogeneous materials, and the analysis and design/control of devices made of heterogeneous materials.

In the current work, the correlation between grain size and texture features was not taken into consideration. Further studies are currently being conducted to address this issue.

Acknowledgments

The senior author (N. Zabaras) acknowledges support from the Computational Mathematics program of AFOSR (grant F49620-00-1-0373), the DOE Office of Science ASCR (award DE-SC0004910), the Materials Design and Surface Engineering program of the NSF (award CMMI-0757824), the Mechanical Behavior of Materials program Army Research Office (proposal to Cornell University No. W911NF0710519) and an OSD/AFOSR MURI09 award to Cornell University on uncertainty quantification.

References

[1] V. Sundararaghavan and N. Zabaras, A statistical learning approach for the design of polycrystalline materials, Statistical Analysis and Data Mining, 1 (2009), 306–321.
[2] V. Sundararaghavan and N. Zabaras, Design of microstructure-sensitive properties in elasto-viscoplastic polycrystals using multi-scale homogenization, Int. J. Plast., 22 (2006), 1799–1824.
[3] S. Sankaran and N. Zabaras, Computing property variability of polycrystals induced by grain size and orientation uncertainties, Acta. Mater., 55 (2007), 2279–2290.
[4] N. Zabaras and S. Sankaran, An information-theoretic approach to stochastic materials modeling, IEEE Computing in Science and Engineering (CiSE) (special issue of "Stochastic Modeling of Complex Systems", D. M. Tartakovsky, and D. Xiu, edts), Mar/Apr (2007), 50–59.
[5] B. Ganapathysubramanian and N. Zabaras, Modelling diffusion in random heterogeneous media: data-driven models, stochastic collocation and the variational multi-scale method, J. Comput. Phys., 226 (2007), 326–353.
[6] B. Ganapathysubramanian and N. Zabaras, A non-linear dimension reduction methodology for generating data-driven stochastic input models, J. Comput. Phys., 227 (2008), 6612–6637.
[7] R. C. Frank, Orientation mapping, Met. Trans. A., 19A (1988), 403–408.
[8] S. Acharjee and N. Zabaras, A proper orthogonal decomposition approach to microstructure model reduction in Rodrigues space with applications to optimal control of microstructure-sensitive properties, Acta. Mater., 51 (2003), 5627–5646.
[9] S. Ganapathysubramanian and N. Zabaras, Design across length scales: a reduced-order model of polycrystal plasticity for the control of microstructure-sensitive material properties, Comput. Meth. App. Mech. Eng., 193 (2004), 5017–5034.
[10] B. Kouchmeshky and N. Zabaras, The effect of multiple sources of uncertainty on the convex hull of material properties of polycrystals, Comput. Mater. Sci., 47 (2009), 342–352.
[11] X. Ma and N. Zabaras, An adaptive hierarchical sparse grid collocation algorithm for the solution of stochastic differential equations, J. Comput. Phys., 228 (2009), 3084–3113.
[12] A.W. Bowman and A. Azzalini, Applied Smoothing Techniques for Data Analysis, Oxford University Press, 1997.

[13] J. T. Kent, J. M. Bibby, and K. V. Mardia, Multivariate Analysis, Probability and Mathematical Statistics, Elsevier, 2006.
[14] S. T. Roweis and L. K. Saul, Nonlinear dimensionality reduction by locally linear embedding, Sci., 290 (2000), 2323–2326.
[15] V. deSilva and J. B. Tenenbaum, Global versus local methods in nonlinear dimensionality reduction, Adv. Neural. Inform. Pro. Syst., 15 (2003), 721–728.
[16] J. Tenenbaum, V. de Silva, and J. Langford, A global geometric framework for nonlinear dimension reduction, Sci., 290 (2000), 2319–2323.
[17] A Global Geometric Framework for Nonlinear Dimensionality Reduction, freely downloadable software available at `http://isomap.stanford.edu/`.
[18] C. E. Krill III and L.-Q. Chen, Computer simulation of 3-D grain growth using a phasefield model, Acta. Mater., 50 (2002), 3059–3075.
[19] S. Sankaran and N. Zabaras, A maximum entropy approach for property prediction of random microstructures, Acta. Mater., 54 (2006), 2265–2276.
[20] D. Fan and L.-Q. Chen, Computer simulation of grain growth using a continuum field model, Acta. Mater., 45 (1997), 611–622.
[21] D. Fan, C. Geng, and L.-Q. Chen, Computer simulation of topological evolution in 2-D grain growth using a continuum diffuse-interface field model, Acta. Mater., 45 (1997), 1115–1126.
[22] S. Vedantam and B. S. V. Patnaik, Efficient numerical algorithm for multiphase field simulations, Phys. Rev. E., 73 (2006), 016703.
[23] E. L. Melnick and A. Tenenbein, Misspecifications of the normal distribution, Am. Stat., 36(4) (1982), 372–373.
[24] M. Rosenblatt, Remarks on a multivariable transformation, Ann. Math. Stat., 23 (1952), 470–472.
[25] X. Yue and W. E, The local microscale problem in the multiscale modeling of strongly heterogeneous media: effects of boundary conditions and cell size, J. Comput. Phys., 222 (2007), 556–572.
[26] S. Kumar and R. N. Singh, Thermal conductivity of polycrystalline materials, J. Am. Ceram. Soc., 78(3) (1995), 728–736.